Decadal Variability of the Tropical Atlantic Ocean Surface Temperature in Shipboard Measurements and in a Global Ocean–Atmosphere Model

VIKRAM M. MEHTA

Universities Space Research Association, Laboratory for Atmospheres, NASA/Goddard Space Flight Center, Greenbelt, Maryland

THOMAS DELWORTH

NOAA/Geophysical Fluid Dynamics Laboratory, Princeton, New Jersey

(Manuscript received 2 July 1993, in final form 20 April 1994)

ABSTRACT

Numerous analyses of relatively short (25–30 years in length) time series of the observed surface temperature of the tropical Atlantic Ocean have indicated the possible existence of decadal timescale variability. It was decided to search for such variability in 100-yr time series of sea surface temperature (SST) measured aboard ships and available in the recently published Global Ocean Surface Temperature Atlas (GOSTA). Fourier and singular spectrum analyses of the GOSTA SST time series averaged over 11 subregions, each approximately 1 $\times 10^6$ km^2 in area, show that pronounced quasi-oscillatory decadal ($\sim$8–20 yr) and multidecadal ($\sim$30–40 yr) timescale variability exists in the GOSTA dataset over the tropical Atlantic.

Motivated by the above results, SST variability was investigated in a 200-yr integration of a global model of the coupled oceanic and atmospheric general circulations developed at the Geophysical Fluid Dynamics Laboratory (GFDL). The second 100 yr of SST in the coupled model's tropical Atlantic region were analyzed with a variety of techniques. Analyses of SST time series, averaged over approximately the same subregions as the GOSTA time series, showed that the GFDL SST anomalies also undergo pronounced quasi-oscillatory decadal and multidecadal variability but at somewhat shorter timescales than the GOSTA SST anomalies. Further analyses of the horizontal structures of the decadal timescale variability in the GFDL coupled model showed the existence of two types of variability in general agreement with results of the GOSTA SST time series analyses. One type, characterized by timescales between 8 and 11 yr, has high spatial coherence within each hemisphere but not between the two hemispheres of the tropical Atlantic. A second type, characterized by timescales between 12 and 20 yr, has high spatial coherence between the two hemispheres. The second type of variability is considerably weaker than the first. As in the GOSTA time series, the multidecadal variability in the GFDL SST time series has approximately opposite phases between the tropical North and South Atlantic Oceans. Empirical orthogonal function analyses of the tropical Atlantic SST anomalies revealed a north–south bipolar pattern as the dominant pattern of decadal variability. It is suggested that the bipolar pattern can be interpreted as decadal variability of the interhemispheric gradient of SST anomalies.

The decadal and multidecadal timescale variability of the tropical Atlantic SST, both in the actual and in the GFDL model, stands out significantly above the background "red noise" and is coherent within each of the time series, suggesting that specific sets of processes may be responsible for the choice of the decadal and multidecadal timescales. Finally, it must be emphasized that the GFDL coupled ocean–atmosphere model generates the decadal and multidecadal timescale variability without any externally applied force, solar or lunar, at those timescales.

1. Introduction

The natural variability of the climate system at multiyear to decadal (defined for the current work as 8–20 yr) timescales has received increased attention over the last two decades. It is important to study this natural variability both in its own right and for its implications for the detection of climate change.

In studying multiyear to decadal timescale variability of the coupled ocean–atmosphere system, the Atlantic region has been the subject of numerous studies, primarily because of the availability of relatively long observational records of various quantities. Since shipboard measurements were the primary source of information about sea surface temperature (SST) until the advent of earth-orbiting satellites, spatial coverage of long observational records containing reliable measurements is dependent upon and limited by locations of shipping routes. Only 25–30-yr records of SST, for example, are available at relatively high spatial resolution covering extensive areas of the tropical Atlantic Ocean. Using these observational records, a number of studies (see, for example, Weare 1977; Hastenrath 1978, 1990; Lough 1986; Folland et al. 1986; Semazzi

Corresponding author address: Dr. Vikram M. Mehta, Laboratory for Atmospheres, NASA/Goddard Space Flight Center, Greenbelt, MD 20771.

et al. 1988; Nicholson and Nyenzi 1990; and Servain 1991), primarily using empirical orthogonal function (EOF) analyses, have demonstrated the existence of SST variability in the tropical Atlantic at multiyear timescales. The more recent of the above analyses have also provided some evidence of decadal timescale variability. In the above analyses of relatively short SST time series on a regular spatial grid, the mode of variability that has attracted the most attention is the second EOF of the tropical Atlantic SST anomalies. This mode has nearly constant amplitude with respect to longitude in the tropical Atlantic basin and opposite signs on the two sides of the equator, with the maximum amplitudes at approximately 15°N and 15°S latitudes. The associated time series usually exhibits variability at timescales of a few years to a decade with the maximum amplitude of approximately 1 K. The north–south cross-equatorial pattern has been characterized by some researchers as a dipole or a seesaw. The same type of cross-equatorial pattern of SST variability appears as the second EOF in Ward and Folland's (1991) analyses of 80-yr time series of shipboard SST measurements, compiled by Bottomley et al. (1990), accumulated in 10° lat × 10° long grid boxes from 60°S to 60°N in the Atlantic region. Recently, Houghton and Tourre (1992) have questioned the physical interpretation of the dipole or seesaw variability in the tropical Atlantic SST anomalies and used rotated EOF analysis to show that SSTs in the tropical Atlantic undergo independent interannual variabilities on the two sides of the equator.

Variability of other climate quantities in the tropical Atlantic region has also been associated with the earlier described SST variability. Folland et al. (1986, 1991), Semazzi et al. (1988), Hastenrath (1990), and Ward and Folland (1991), among others, have found correlations between African rainfall variability and the tropical Atlantic SST variability. Moura and Shukla (1981) calculated correlation coefficients between the tropical Atlantic SST and rainfall over northeast Brazil during 1948–72 and showed that the most severe drought events during this period were associated with the simultaneous occurrence of warm SST anomalies over the tropical North Atlantic and cold SST anomalies over the tropical South Atlantic.

Motivated by their findings of statistical relationships, Folland et al. (1986) and Moura and Shukla (1981) have explored physical relationships between the tropical Atlantic SST variability and rainfall variability over the Sahel region of Africa and over Brazil, respectively, with the help of atmospheric general circulation models (GCMs). Although the atmospheric GCMs' responses to prescribed tropical Atlantic SST anomalies agree reasonably well with the observed rainfall patterns over the Sahel and northeast Brazil, such experiments cannot explain why there is multiyear to decadal timescale variability in the tropical Atlantic SST. Since the tropical Atlantic SST variability is linked to climate variability over the tropical Atlantic Ocean, over the adjacent continental regions, and, perhaps, over other parts of the world, it is very important to understand the cause(s) of the SST variability not only to satisfy intellectual curiosity but also to possibly predict various phases of the climate variability.

As the earlier described studies of SST variability show, there is consensus that there is variability in the tropical Atlantic SST at timescales of a few years to a decade. There is controversy, however, about the north–south structure of the SST variability. Moreover, because of the relatively short time series used in all except one of these studies, the significance and spatial structure of *decadal* timescale SST variability cannot be reliably ascertained. Since long (approximately 100 yr and longer) time series of SST measurements over large areas of the tropical Atlantic, especially in the Southern Hemisphere, are not available, it is not currently possible to extract detailed and accurate information about the strength and spatial structures of decadal variability of tropical Atlantic SST from observational records. There are, however, SST time series spanning periods longer than 100 yr, compiled by Bottomley et al. (1990) from shipboard measurements (hereafter referred to as the observed SST), available for a few locations situated on shipping routes in the tropical Atlantic Ocean. One goal of the present work was to find out if the available 100-yr observed SST time series contain significant decadal timescale variability.

In addition to the indications from the earlier described observational studies, modeling work (Mehta 1991, 1992, 1994) with idealized ocean–atmosphere models has suggested that normal modes of oscillation of oceanic, atmospheric, or coupled oceanic–atmospheric mean meridional circulations can generate decadal timescale variability in the tropical Atlantic region climate. Therefore, the other goal of the present work was to find out if decadal variability in the tropical Atlantic SST exists in a model of the global coupled oceanic and atmospheric general circulations developed at the Geophysical Fluid Dynamics Laboratory (GFDL). Specifically, the following questions were addressed to the observed and model SST datasets. Do 100-yr time series of SST based on ship observations contain significant decadal timescale variability in the tropical Atlantic region? What is the phase relationship between the decadal variabilities in the northern and southern tropical Atlantic SST? Do the time series of tropical Atlantic SST in the GFDL coupled model contain significant decadal timescale variability? What is the spatial structure of decadal timescale variability of SST in the GFDL coupled model?

A brief description of the observed SST dataset is given in section 2, the ocean and atmosphere models are described in section 3, and data analysis techniques are given in section 4. Results of analyses of SST vari-

ability are described in sections 5 and 6. Concluding remarks are presented in section 7.

2. The GOSTA SST dataset

The Global Ocean Surface Temperature Atlas (GOSTA) spanning the period 1856–1989 has been compiled by Bottomley et al. (1990) from ship observations. Since measurement techniques have changed over this period, estimated corrections to the measured SST are also available in the same dataset. Both original and corrected SST time series were used in the present work. In the time series analyzed in the present study, typical corrections consist of 0.4–0.5 K additions to the uncorrected SST before 1941. The monthly average SST anomalies (with respect to the 1951–1980 climatology of each time series) are available on a regular 5° lat × 5° long grid. The monthly average anomalies were averaged to form annual averages subject to the criterion that four or more monthly observations be available for each year. Years in which the criterion was not met were regarded as not having any data. After the annual averaging, time series from four adjacent grid boxes were averaged. (The four grid boxes represent an area of approximately 1×10^6 km^2) Enough observations were found to form annual-average time series over 11 such 10° lat × 10° long subregions all but two of which are completely nonoverlapping in the area of interest over the tropical Atlantic. For years in which none of the four grid boxes had observations, an SST anomaly value was assigned by linear interpolation from adjacent years. Locations of the 11 subregions are shown in Fig. 1. Anomalies for the period 1889–1988 have been used in the present work. Anomaly time series in grid boxes 1–9 in Fig. 1 had less than or equal to three consecutive years with missing SST anomalies and the maximum number of missing anomalies in the nine time series was eight. The time series for grid boxes 10 and 11 had four and six consecutive years, respectively, with missing SST anomalies, and had 10 and 13 missing anomalies, respectively, during the 100-yr analysis period.

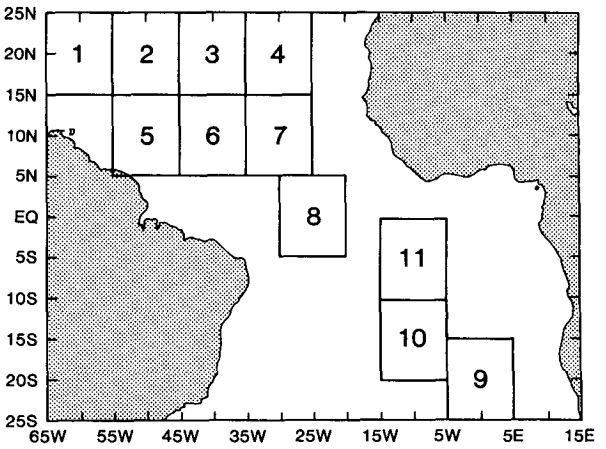

FIG. 1. Locations of the GOSTA subregions in the tropical Atlantic, within each of which 100-yr time series of observed SST were averaged.

3. Models and experiment

a. Model description

The coupled ocean–atmosphere model used for this study consists of a general circulation model of the world oceans coupled to a general circulation model of the global atmosphere. The coupled ocean–atmosphere model was described by Manabe et al. (1991).

In the atmospheric component (Gordon and Stern 1982) of the coupled model, the equations of mass, momentum, thermodynamic energy, and atmospheric moisture are integrated using the spectral Galerkin method (see, for example, Orszag 1970). In this formulation, the horizontal distribution of a predicted variable is represented by a rhomboidally truncated series of spherical harmonics containing 15 zonal waves and 15 associated Legendre polynomials corresponding to an approximate resolution of 4.5° in lat and 7.5° in long. A finite-difference formulation is used in the vertical, with nine unequally spaced levels. The effects of clouds, water vapor, carbon dioxide, and ozone are included in the calculation of solar and terrestrial radiation. Moist convective adjustment is used to remove moist static instability in the model atmosphere. Water vapor and precipitation are predicted in the model but a constant mixing ratio of carbon dioxide and zonally uniform distribution of ozone are prescribed. Overcast cloud is assumed whenever relative humidity exceeds a threshold value. Otherwise, clear sky is predicted. Heat, water, and snow budgets at the continental surface are included in the model.

The basic structure of the oceanic component of the coupled model is similar to the model described by Bryan and Lewis (1979). Equations of mass, momentum, thermodynamic energy, and salinity are integrated on a finite-difference grid that has a spacing of 4.5° lat and 3.7° long between grid points. The grid has 12 levels in the vertical direction. In addition to the horizontal and vertical background mixing, subgrid-scale mixing, and convective overturning, the model has isopycnal mixing as discussed by Bryan (1987). The model predicts sea ice using a simple model developed by Bryan (1969).

The atmospheric and oceanic components interact with each other through the exchanges of heat, freshwater, and momentum fluxes at the air–sea interface. The freshwater flux includes runoff from the continents. Seasonally varying insolation is the external force driving the coupled ocean–atmosphere model.

When the time integration of a model starts from an initial condition that is not in equilibrium, the model climate usually undergoes a drift toward an equilibrium state. Such a drift contaminates the natural

variability of the model climate that is the subject of the present study. Thus, it is highly desirable that the initial condition for the time integration be as close to the equilibrium state as possible. Manabe and Stouffer (1988) have shown that a time integration of the original version of the coupled model yielded an unrealistic equilibrium state, characterized by an exaggerated halocline at high latitudes and the absence of a substantial thermohaline circulation in the North Atlantic. To offset this bias of the model, they adjusted the flux of freshwater at the oceanic surface by an amount that varies geographically and seasonally but does not change during the integration of the coupled model. Performing this adjustment, they obtained two stable equilibria with and without a thermohaline circulation of substantial intensity in the Atlantic Ocean, depending on the initial condition chosen. The equilibrium obtained with flux adjustment resembles the current condition in the Atlantic Ocean with a substantial thermohaline circulation. In the present experiment, the adjustment was performed for both freshwater and heat fluxes at the ocean surface. The *seasonal* and *geographical distributions* of the *adjustment* did not have *interannual variations* and did not depend on the *surface anomalies* of temperature and salinity. Thus, the adjustments did not explicitly affect the feedback processes that reduce these anomalies. Details of the flux adjustment technique and magnitudes of flux adjustments are described in Manabe et al. (1991).

Starting from a state in quasi equilibrium, the coupled model was integrated for 200 yr of model time. The analyses presented in this paper have used the model output from years 101 to 200.

b. *Stability of model climate*

When analyzing variability of the modeled climate, it is important and can be instructive to assess how well the model can simulate the long-term climate and the seasonal cycle. Often, variability of the modeled climate is a function of the model climate and/or the seasonal cycle. Therefore, accurate simulations of the long-term climate and the seasonal cycle might be prerequisites for accurate simulations of climate variability.

Averages of January and July SST in the GFDL coupled model over the 100-year period of the analyses are shown in Fig. 2. Comparison of Fig. 2 with Levitus's (1982) averages of the observed January and July SST shows that the simulated SST has similar magnitudes and patterns as the observed SST.

Properties of the numerical methods used in the model, computational errors, and long-term variability are some of the major sources of drift in the model climate away from the present climate even if all external forces are held constant or, at the most, have constant annual cycles. In addition to successfully simulating the long-term climate, it is desirable that there

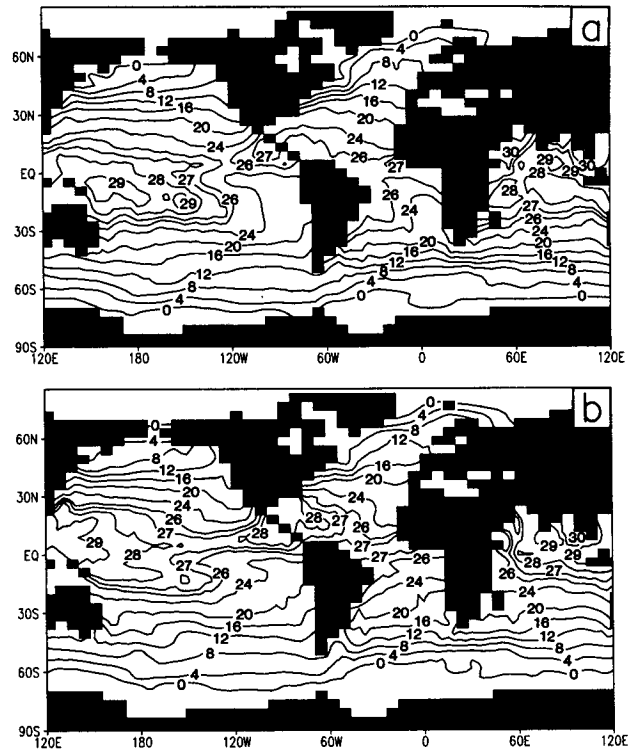

FIG. 2. The 100-yr average sea surface temperature (°C) from the GFDL coupled ocean–atmosphere model for (a) January and (b) July.

be no long-term drift in the model climate. If present, the long-term drift can interfere with the existence, detection, and physical interpretation of periodic or quasi-periodic climate variability. A measure of the stability of the GFDL coupled model is the variability of globally averaged SST (Fig. 3a) over the analysis period. The maximum peak-to-peak amplitude of globally averaged SST in Fig. 3a is 0.2 K. Even though the globally averaged SST undergoes variability at various timescales, a linear trend fitted to the 100-yr time series is only −0.0022 K/100 yr. Another measure of the stability of model SST is the linear trend of the annual-mean SST time series at each grid point in the tropical Atlantic region. Figure 3b shows contours of the slope of the fitted line at each grid point. During the 100-yr period of the analyses, SST decreases over extensive areas of the tropical Atlantic Ocean. Between 30°S and 30°N, the maximum magnitude of the slope is only 0.25 K/100 yr, with the SST decreasing at most of the grid points at 0.05–0.1 K/100 yr. Thus, adjustments of the freshwater and heat fluxes appear to keep the GFDL coupled model reasonably stable and the long-term model climate reasonably close to the observed climate over the 100-yr period of the analysis.

4. Analysis techniques

We used a variety of time series analysis techniques to study variability of the tropical Atlantic SST. The

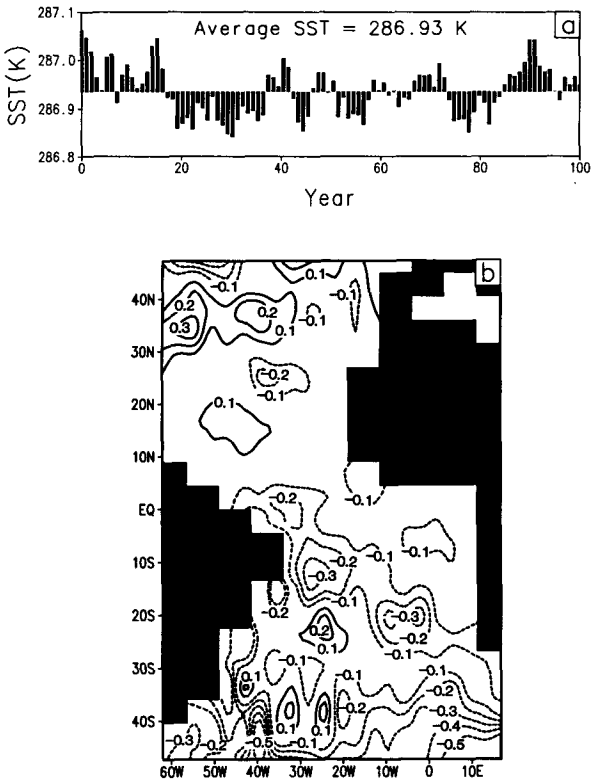

FIG. 3. (a) Time series of globally averaged sea surface temperature (K) from the GFDL coupled ocean–atmosphere model during the 100-yr analysis period; (b) linear trends (K/100 yr) in 100-yr sea surface temperature time series in the GFDL coupled model.

Fourier spectrum analysis (FSA), based on the fast Fourier transform technique, was used to estimate spectra of SST time series. Equivalent "red noise" spectra were calculated using the formula derived by Gilman et al. (1963). Using the red noise spectra as reference, statistical significance of the various spectral peaks was estimated by calculating the spectral density that the estimated spectral peaks must exceed to reject a null hypothesis of "red noise" with 99% a priori confidence. The reason for using a priori confidence levels was that because of indications from the earlier described analyses of observations and results from our idealized coupled ocean–atmosphere models, there appeared to be a reasonably high probability that the tropical Atlantic SST would have decadal timescale variability. A statistic based on the number of degrees of freedom in each spectral estimate and the corresponding percentile value for the chi-square distribution was used to calculate the confidence level. Each spectral estimate shown in this paper has approximately five degrees of freedom. Cross spectra of pairs of SST time series were estimated from the Fourier transforms of the cross-covariance function of the time series. Squared coherence and phase difference between the time series at each Fourier frequency were then calculated from the spectra and cross spectra of the time series. The 95% and 99% confidence levels on the estimated squared coherence were calculated using the formula developed by Bloomfield (1976).

We used singular spectrum analysis (SSA) to verify and complement the results obtained with FSA. Vautard and Ghil (1989) and Penland et al. (1991) have provided mathematical details of the SSA technique, so only a brief description is given here. In the SSA technique, the basis functions, in terms of which the original time series are decomposed, are determined from the time series itself, using several lagged copies of the time series in an EOF analysis. The eigenvalues and eigenvectors of the matrix formed by covariances among the lagged copies of the time series are calculated and then the time series is projected onto the eigenvectors to calculate principal components. Since the eigenvectors and the principal components (PCs) in SSA are functions of time, they are usually referred to as T-EOFs and T-PCs, respectively. The T-EOFs and T-PCs can be combined to reconstruct any subset of components of the original time series. Thus, application of SSA yields data-adaptive coherent structures as in space–time EOF analysis. In SSA, each pair of high-variance eigenvalues is sometimes observed (Vautard and Ghil 1989) to represent a fundamental oscillation, with the two corresponding T-EOFs in quadrature with each other.

We used space–time EOF analyses to isolate large-scale, dominant, coherent structures of SST variability. In addition to the conventional EOF analysis (hereafter referred to as E1), for better interpretation of the results of our analyses, we also used another formulation of the space–time EOF analysis technique in which the covariance (or correlation) matrix is constituted by covariances (or correlation coefficients) between spatial patterns at pairs of times rather than between time series at two grid points in space as in the conventional EOF analysis. In this formulation, the size of the covariance (or correlation) matrix is equal to the number of points in time rather than in space. Since usually the number of points in time is considerably smaller than the number of points in space, the size of the operator matrix in our formulation is smaller than in conventional EOF analysis. Eigenvectors of the covariance (or correlation) matrix are EOF time series, and PCs are formed by projecting the original SST anomaly time series at each grid point onto each EOF. In this formulation, PCs are spatial patterns. Two slightly different variations of this EOF analysis technique were used. In one variation (hereafter referred to as E2) the domain-average anomaly is not subtracted from the SST anomaly at each grid point before computing covariances between anomaly maps at pairs of times. In the other variation (hereafter referred to as E3) the domain-average anomaly is subtracted from

the SST anomaly at each grid point to analyze the variability of gradients of anomalies. The influence of the domain average on interpretation of our results is discussed later. Distinctness of eigenvalues and the consequent orthogonality of the corresponding eigenvectors obtained by the above three techniques was estimated with the formula developed by North et al. (1982) based on sampling errors in the data. Statistical significance of correlation coefficients was estimated using the t statistic (Spiegel 1961) based on the Student's t distribution.

5. Analysis of SST time series at selected subregions

As described in section 2, 100-yr long, annual average, original and corrected SST anomaly time series over 11 subregions of the tropical Atlantic region were selected from the GOSTA dataset. Linear trends of SST anomaly series versus time were computed and removed from the time series at each grid point. The slopes and intercepts of the linear trends in the corrected time series are given in Table 1. Since the anomalies have been calculated with respect to the average SST during the period 1951–1980 in each grid box, the straight-line regressions have nonzero intercepts. Some of the time series show gradual rises in SST, with a maximum increase of approximately 1 K over the 100-yr period in the box spanned by 15°–25°S, 5°W–5°E. Visual inspection of the time series suggests that the long-term trends are not constant within a time series and that there are episodes of slower or faster rises. The original time series have several abrupt changes in the levels of the anomalies, most notably around 1940. There are several possible causes of the linear trends in the observed SST time series: (a) inaccuracies in measurement, (b) errors in the correction procedure, (c) disruptions in measurement/compilation due to wars, and (d) changes in surface temperature of the tropical Atlantic Ocean since 1889. Discussion of the possible causes of the linear trends is beyond the scope of the present paper.

TABLE 1. Coefficients of linear regression between time and observed SST.

Grid box	Slope (K/100 yr)	Intercept (K)
1. 15°–25°N, 55°–65°W	0.24	−0.20
2. 15°–25°N, 45°–55°W	0.28	−0.24
3. 15°–25°N, 35°–45°W	0.36	−0.27
4. 15°–25°N, 25°–35°W	0.34	−0.27
5. 5°–15°N, 45°–55°W	0.32	−0.31
6. 5°–15°N, 35°–45°W	0.14	−0.10
7. 5°–15°N, 25°–35°W	0.23	−0.16
8. 5°S–5°N, 20°–30°W	0.58	−0.36
9. 15°–25°S, 5°W–5°E	0.93	−0.69
10. 10°–20°S, 5°–15°W	0.70	−0.50
11. 0°–10°S, 5°–15°W	0.16	−0.31

a. Fourier spectrum analysis

To obtain a representative spectrum for each latitude band and increase the signal-to-noise ratio, the corrected and original (uncorrected) GOSTA SST time series, along with the GFDL model SST time series, were averaged over the subregions defined in Table 1. There are four subregions averaged together in the latitude band 15°–25°N and three subregions in the latitude band 5°–15°N (see Fig. 1). Spectra of the averaged time series in each of the above two latitude bands, as well as in the latitude bands 5°S–5°N, 0°–10°S, 10°–20°S, and 15°–25°S, were estimated with the highest possible Fourier frequency resolution. The spectra of the averaged GFDL SST and corrected GOSTA SST time series are shown in Fig. 4. Each spectral estimate in Fig. 4 has approximately five degrees of freedom. Using the equivalent red noise spectrum and the 99% confidence level as references, one can see that all six spectra of the averaged GOSTA SST time series have significant peaks at decadal timescales. The spectra of the corresponding GFDL SST time series also have significant peaks at decadal timescales. Both groups (GOSTA and GFDL) of spectra contain peaks at multidecadal and other timescales also. Even though only one (b and h) of the six pairs of spectra contain significant peaks at exactly the same Fourier frequencies, the presence of decadal timescale peaks in both groups is unmistakable. Spectral density of the significant decadal peaks is approximately four to five times greater in the Southern Hemisphere than in the Northern Hemisphere. (Note that the spectral density scales are different in Figs. 4d,e.) In both hemispheres, total variance and spectral density of significant decadal peaks are maximum at approximately 15° latitude. In the spectra of the GFDL SST time series the dominant decadal peaks are centered almost at the 10-yr period in both hemispheres.

The variance of each of the time series is also shown in Fig. 4. The variances of the GOSTA SST and the corresponding GFDL SST time series are quite comparable in four of the six pairs. At approximately 10°N and 10°S, the total variances of the GOSTA SST time series are approximately twice as large as the total variances of the GFDL SST time series. Although the total variance of the model SST time series is approximately twice as large in the Southern Hemisphere as in the Northern Hemisphere, the spectral density of the significant decadal peaks is approximately the same in both hemispheres. As for the GOSTA spectra, the total variance and spectral density of the significant decadal peaks in the GFDL spectra are maximum near 15°S. Unlike the GOSTA spectra, the total variance and spectral density of the significant decadal peaks in the GFDL model continue to increase north of 15°N.

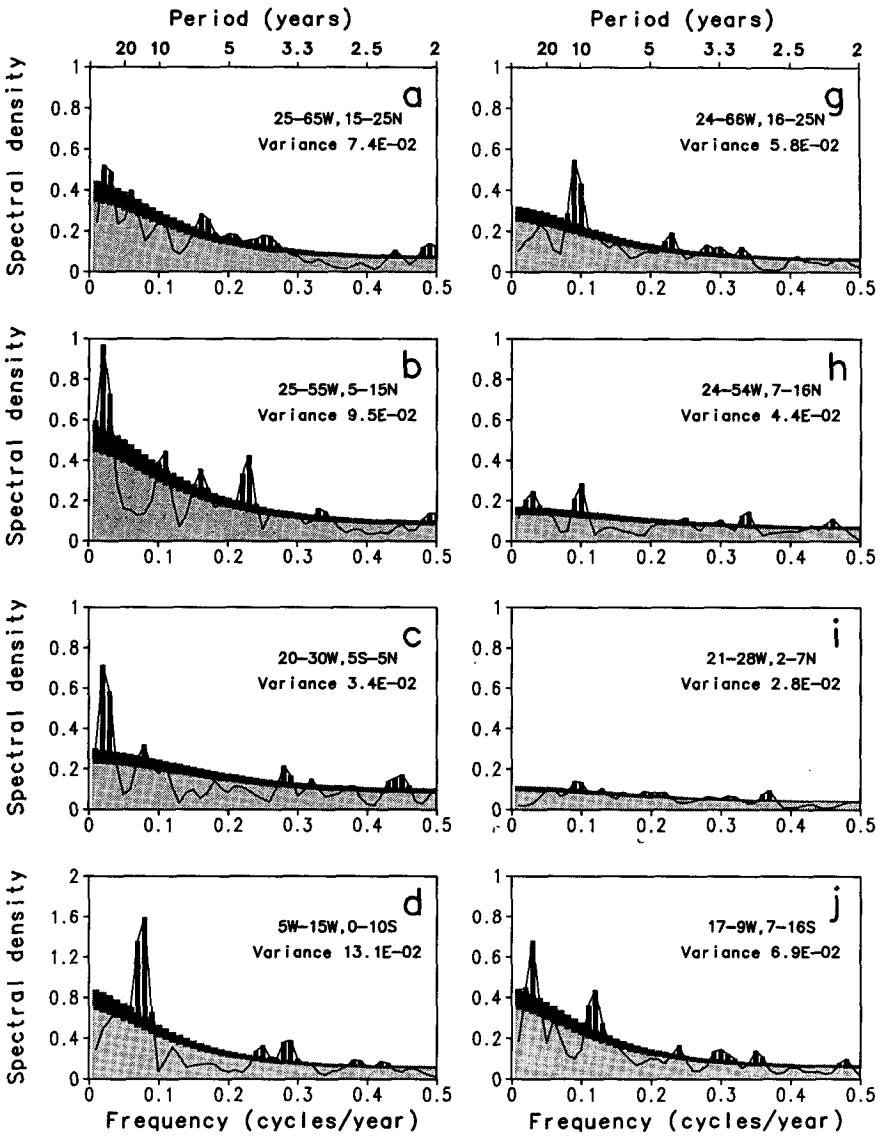

FIG. 4. Fourier spectra of SST time series for six subregions in the tropical Atlantic region. Locations and variance of the SST time series of each subregion are given in each box. Annual-average corrected time series were used to estimate spectra. The solid line is the estimated spectrum of the grid box time series, lighter shading denotes the equivalent red noise spectrum, darker shading denotes the red noise spectrum that spectral estimates must exceed for significance at the 99% level. The significant spectral estimates are shown by black bars. All spectral estimates are in K^2 per unit frequency. Panels (a)–(f) show spectra of the observed GOSTA SST time series, and (g)–(l) show spectra of the SST time series from the GFDL coupled model.

Spectra (not shown) of the averaged original (uncorrected) GOSTA SST time series were found to be generally similar to the corresponding spectra of the corrected time series, with both sets of spectra containing peaks at decadal timescales. Variances are significantly larger in the original time series than in the corrected time series, which may be because of abrupt shifts in the levels of the original time series in approximately 1940. The corrections applied for changes in measurement technique apparently preserve the basic spectral characteristics of the GOSTA time series used in this work.

Spectra of the corrected GOSTA SST time series were also estimated with Fourier frequency resolution three times coarser than the highest possible resolution. Significant spectral peaks at decadal timescales are also present in the coarse-resolution spectra (not shown). As subsequent discussion in this paper shows, two types of spatial structures of the tropical Atlantic SST variability appear to exist within the decadal timescale

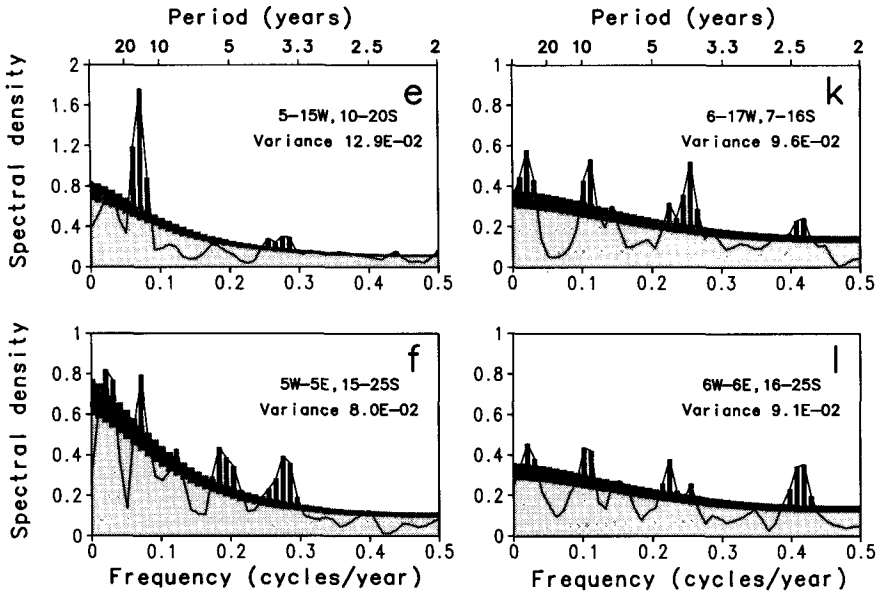

FIG. 4. (*Continued*)

band. Therefore, to achieve the resolution necessary to distinguish between these two types of variability, spectral and cross-spectral analyses were performed on the GOSTA and GFDL SST time series at the highest possible Fourier frequency resolution.

To obtain a better indication about the spatial distribution of decadal timescale SST variability, spectra of the 11 corrected GOSTA SST time series were estimated after removal of the linear trend in each time series. Nine out of the 11 spectra (not shown) have significant peaks at decadal timescales. In the 5°–15°N and 15°–25°N latitude bands, spectral peaks at decadal timescales are stronger in the western part of the basin. Spectra (not shown) of the original (uncorrected) GOSTA time series have generally similar characteristics. For comparison, the SST time series from the GFDL coupled model were averaged over the corresponding 11 subregions. Significant decadal-scale variability is clearly present in the spectra of the 11 GFDL SST time series. To analyze the east–west distribution of the decadal variability in a systematic manner, 10 subregions, each of which spanned approximately 10° lat × 10° long, were selected from the GFDL SST dataset. These subregions were in the western and eastern parts of the tropical Atlantic Ocean at five latitude bands. Spectra (not shown) of the 10 averaged time series show that significant decadal timescale variability of SST in the GFDL coupled model exists in the western and central tropical North Atlantic and the eastern tropical South Atlantic. All but one of the GOSTA SST spectra have significant peaks at multidecadal (~30–40 yr) timescales as do four of the six GFDL SST spectra. Since the SST time series span only 100 yr, not much physical significance would be attached to peaks near the lowest resolvable frequency in a Fourier spectrum analysis. However, the singular spectrum analysis of these datasets, discussed in the next subsection, also reveals the presence of coherent multidecadal variability in the GOSTA and GFDL SST time series.

b. Singular spectrum analysis

Unlike the Fourier spectrum analysis, basis functions in the singular spectrum analysis are derived empirically from the time series being analyzed, using many lagged copies of the time series in an EOF analysis. Each lagged copy, called a "window," spans a segment of the time series. The EOF-based SSA isolates the dominant coherent modes of variability in the time series. The SSA technique is thus fully data adaptive and was used in this work to verify the FSA results discussed in the previous subsection.

The choice of a window width for SSA is subjectively based on the timescales one is interested in, the length of the time series, and the nature and quantity of noise in the time series. As discussed by Ghil and Vautard (1991), the optimum window width is the result of a subjective compromise between significant information and statistical confidence. We applied the SSA technique to the six averaged GOSTA and the corresponding six averaged GFDL SST anomaly time series for window widths between 20 and 50 yr. Eigenvalue spectra of the 12 time series, calculated at window widths of 30 yr, are shown in Fig. 5. The eigenvalue spectra, T-EOFs, and T-PCs calculated at other window widths were substantially similar to the results for the 30-yr window width. A comparison (not shown) of the

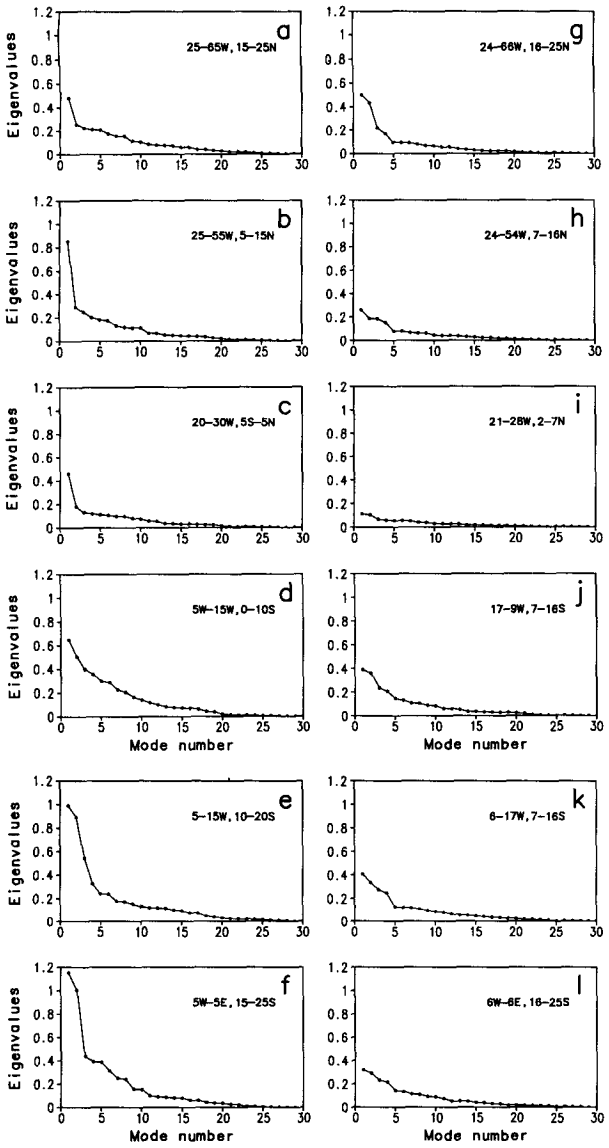

FIG. 5. Eigenvalue spectra from singular spectrum analysis of the SST time series for the same six subregions as in Fig. 4. A 30-yr window width was used. (a)–(f) Spectra of the observed GOSTA SST time series and (g)–(l) spectra of the SST time series from the GFDL coupled model.

eigenvalue spectra for window widths of 20, 30, 40, and 50 yr provides estimates of the noise level in the spectrum of each time series. For each of the 12 time series, approximately the first six to eight eigenvalues were estimated to lie above the noise level.

The first four GOSTA spectra (a, b, c, and d) in Fig. 5 do not show a clean transition from a coherent signal regime to a noise regime. The first eigenvalue dominates the spectrum of each of the first three GOSTA time series. Spectra of the last two GOSTA time series and all of the GFDL time series show an approximate separation between oscillatory signal, represented by single or double eigenvalues, and noise regimes. The T-EOFs representing decadal variability in the GOSTA time series are shown in Fig. 6. The two T-EOFs shown in each box of Fig. 6 are mutually orthogonal. Although there are no T-EOFs for the first three GOSTA time series representing pure oscillations (two approximately equal eigenvalues) at decadal timescales, there are some T-EOFs representing irregular decadal variability as shown in Figs. 6a–c. Therefore, it appears that there is decadal variability of tropical North Atlantic SST anomalies, as found by FSA, but it is buried in a substantial amount of noise, and the SSA technique fails to isolate it cleanly. Based on the SSA spectra alone, indications of decadal timescale SST variability in the tropical North Atlantic cannot be considered statistically significant. The presence of relatively small but statistically significant peaks at decadal timescales in the Fourier spectra (Figs. 4a–c) and the SSA results in Figs. 5a–c and 6a–c together, however, make a strong suggestion of decadal timescale variability of the tropical North Atlantic SST anomalies. In contrast to the tropical North Atlantic, quasi-oscillatory decadal variability, represented by pairs of eigenvalues and T-EOFs in quadrature, is present (Figs. 5d–f and 6d–f) in the tropical South Atlantic GOSTA SST anomalies. The oscillatory decadal variability in the tropical South Atlantic SST anomalies has periods of 12–15 yr in both the SSA and FSA results.

The T-EOFs representing decadal variability in the GFDL SST anomaly time series are shown in Figs. 6g–l. Unlike in the case of the GOSTA SST anomaly time series, all the GFDL SST anomaly time series have pairs of T-EOFs representing oscillatory decadal variability. Inspection of the SSA eigenvalue spectra in Fig. 5 and T-EOFs in Fig. 6 show that the coherent signal and noise regimes are more clearly separated in the GFDL model time series results than in the GOSTA time series results. The SST anomalies in the GFDL-coupled model's tropical North Atlantic clearly undergo oscillatory decadal variability as shown in Figs. 5g–i and 6g–i. The FSA and SSA results for the GFDL model's tropical North Atlantic time series show decadal variability at approximately the same timescales.

Two of the first four T-EOFs from the singular spectrum analysis of all the tropical Atlantic GOSTA and GFDL SST anomaly time series analyzed in this work represent multidecadal oscillations for all window widths between 20 and 50 yr. The two T-EOFs representing multidecadal oscillations in the northernmost and southernmost GOSTA and GFDL model SST anomaly time series are shown in Fig. 7. The GOSTA SST T-EOFs in Figs. 7a,b show irregular oscillations with 30–35 yr periods and the GFDL SST T-EOFs in Figs. 7c,d show irregular oscillations with somewhat shorter periods. The Fourier spectra (Fig. 4) of most of the GOSTA and GFDL time series also have statistically significant peaks at approximately the same timescales indicated by the T-EOFs. A comparison of

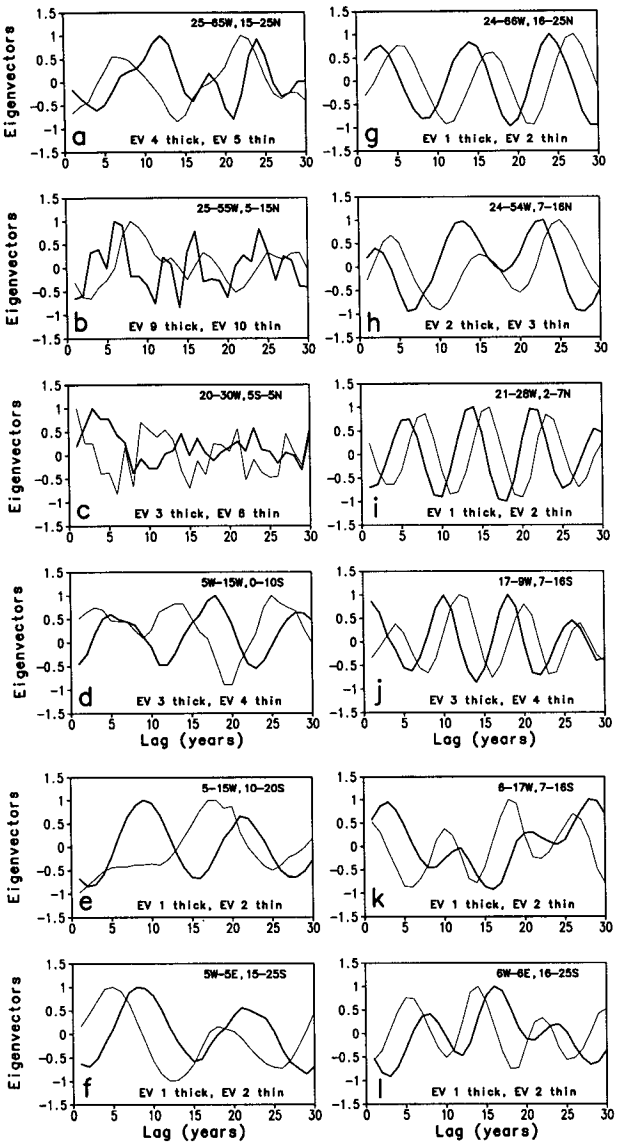

FIG. 6. Eigenvectors representative of decadal variability in the singular spectrum analysis of the SST time series for the same six subregions as in Fig. 4. A 30-yr window width was used. (a)–(f) Eigenvectors for the observed GOSTA SST time series and (g)–(l) eigenvectors for the SST time series from the GFDL coupled model.

the T-EOFs for the northernmost and southernmost subregions suggests that the multidecadal SST variability appears to have approximately opposite phases in the tropical North and South Atlantic. As pointed out in the previous subsection, however, this detection of multidecadal variability in 100-yr time series should not be considered quantitatively definitive.

A reconstruction of the original time series using only a few of the dominant T-EOFs and T-PCs is equivalent to low-pass filtering of the original time series since, in the time series analyzed in this work, the low-frequency variability is isolated by SSA as the dominant modes. To identify periods of pronounced decadal–multidecadal variability of tropical Atlantic SST, the decadal and multidecadal timescale contributions to the GOSTA and GFDL SST anomaly time series, represented by the T-EOFs in Figs. 6 and 7, were reconstructed according to the optimal linear combination technique described by Ghil and Vautard (1991) and Penland et al. (1991). The last 69 years of the reconstructed time series are shown in Fig. 8. T-EOFs and T-PCs calculated with window widths of 30 yr were used in the reconstruction. The variance of the reconstructed time series as a fraction (as percent) of the variance of the original time series is also shown in Fig. 8. In the GOSTA data, decadal–multidecadal timescale variability, as represented by dominant SSA modes, "explains" approximately half the total variance of each SST-anomaly time series. As shown by FSA (Fig. 4) also, the SSA-based reconstructed time series clearly show much stronger decadal–multidecadal timescale variability of the GOSTA SST anomalies in the tropical South Atlantic compared to the tropical North Atlantic. All the original and reconstructed GOSTA time series in Fig. 8 show relatively large decadal timescale anomalies in the 1920s and 1930s, with approximately opposite phases between the tropical North and South Atlantic. During the 1970s also, both the original and reconstructed GOSTA time series show a colder tropical North Atlantic and a warmer tropical South Atlantic. In the GFDL coupled model SST data also, decadal–multidecadal timescale variability "explains" approximately half the total variance of each time series in Figs. 8g–l. In contrast to the GOSTA time series, however, the SSA-based reconstructed GFDL SST time series and the FSA results in Fig. 4 show much stronger decadal variability in the GFDL model's tropical North Atlantic compared to the model's tropical South Atlantic. As in the GOSTA time series, the multidecadal variability in the GFDL time series has approximately opposite phases between the tropical North and South Atlantic.

Thus, two independent spectral analyses of SST measurements between 1889 and 1988 in the tropical Atlantic region show clearly the presence of significant decadal and multidecadal timescale variability. Although generally similar results were obtained from the analyses of SST at the corresponding subregions in the GFDL coupled ocean–atmosphere model, there are small but systematic differences in oscillation timescales and strengths between the two groups of data. The small difference in significant decadal timescales in the northern and southern tropical Atlantic GOSTA spectra suggests that the physical processes giving rise to the decadal variability in the two tropical hemispheres may be related but not identical. The GFDL coupled model simulates decadal variability at virtually the same timescales in the two tropical hemispheres. The GFDL coupled model simulates multidecadal

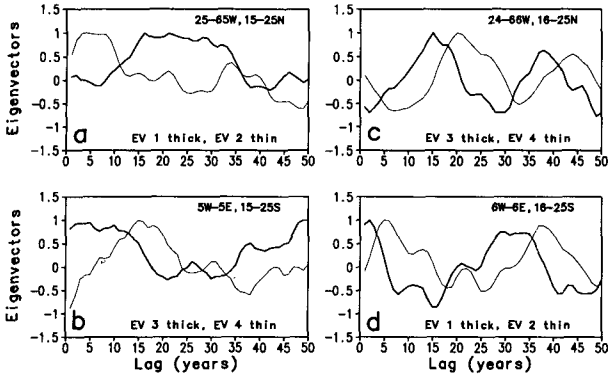

FIG. 7. Eigenvectors representative of multidecadal variability in the singular spectrum analysis of the SST time series for two subregions in the tropical North and South Atlantic Oceans. A 50-yr window width was used. (a)–(b) Eigenvectors for the observed GOSTA SST time series and (c)–(d) eigenvectors for the SST time series from the GFDL coupled model.

variability at somewhat shorter timescales than the multidecadal timescales in the GOSTA SST time series.

c. *Cross-spectral analysis*

To gauge the degree of coherence between the tropical North and South Atlantic decadal variability, we estimated cross spectra, using FSA, between the northern and southern tropical Atlantic time series selecting the GOSTA time series in box 9 (see Fig. 1) as reference. The cross spectra, plotted as squared coherence and phase difference, are shown in Figs. 9a–d. Cross spectra between the corresponding SST time series from the GFDL coupled model were also estimated and are shown in Figs. 9e–h. Each cross-spectral estimate contains approximately five degrees of freedom. The 95% and 99% confidence levels on the squared coherence are also plotted in Fig. 9. The southern and northern tropical Atlantic SST variabilities between approximately 12- and 16-yr periods are highly coherent at the 99% confidence level. In the cross spectra between 15°–25°S and 15°–25°N (Figs. 9a,b,e,f), the squared-coherence peaks in the GOSTA and GFDL SST are at the period of 12.5 yr. The corresponding phase differences are approximately 60°, with the southern tropical Atlantic oscillation leading the northern tropical Atlantic oscillation. In the squared coherence between the GOSTA time series at 15°–25°S and 5°–15°N (Figs. 9c,d), there is a highly coherent peak at the period of 14.3 yr with the corresponding phase difference of approximately 0°. In the squared coherence (Fig. 9g) between the corresponding GFDL SST time series, there is a highly coherent peak at the period of 16.6 yr and a moderately coherent peak at the period of 12.5 yr. The corresponding phase differences (Fig. 9h) are approximately 160° and 60°, respectively, with the Northern Hemisphere 16.6-yr oscillation leading and the Northern Hemisphere 12.5-yr oscillation lagging the respective Southern Hemisphere oscillations.

The spatial distribution of squared coherence and phase difference between the two tropical hemispheres at two timescales within the decadal band are shown in Fig. 10. At a period of 8 yr, the GOSTA SST variability is coherent only within a relatively small area of the tropical South Atlantic, whereas at periods of 12.5 yr and longer there is cross-equatorial coherence with nearly opposite phases between the two tropical hemispheres. Choice of a reference time series in the

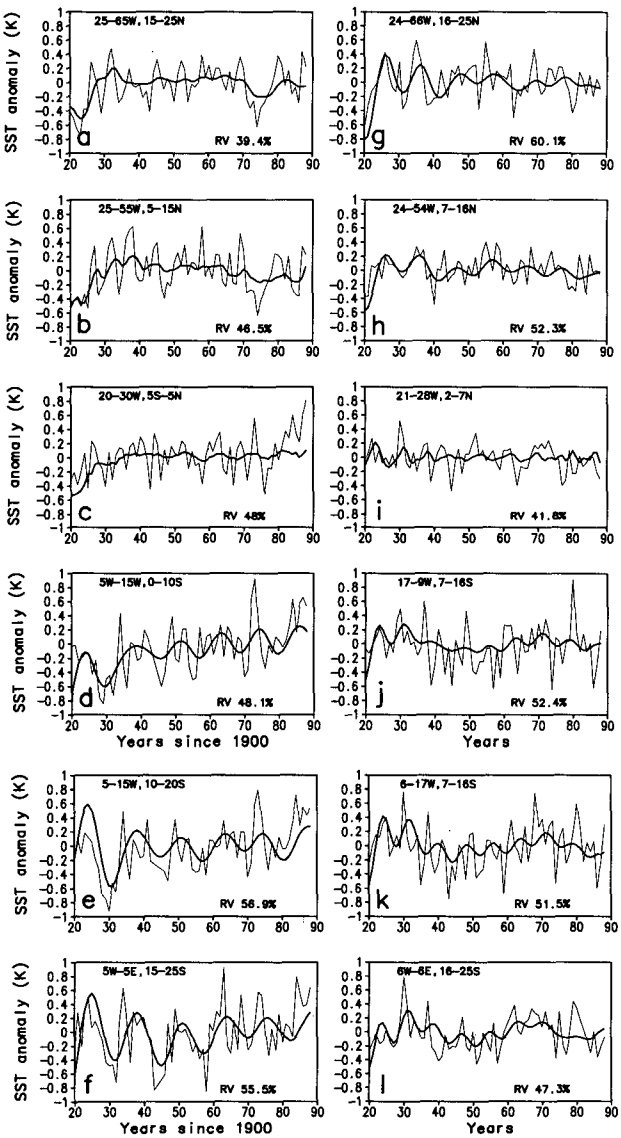

FIG. 8. Original (thin line) and reconstructed (thick line) time series of the observed GOSTA and the GFDL coupled model SST anomalies. The percent variance of reconstructed time series with respect to the variance of the original time series is also given in each box. (a)–(f) Observed GOSTA SST anomaly time series and (g)–(l) the GFDL coupled model SST anomaly time series.

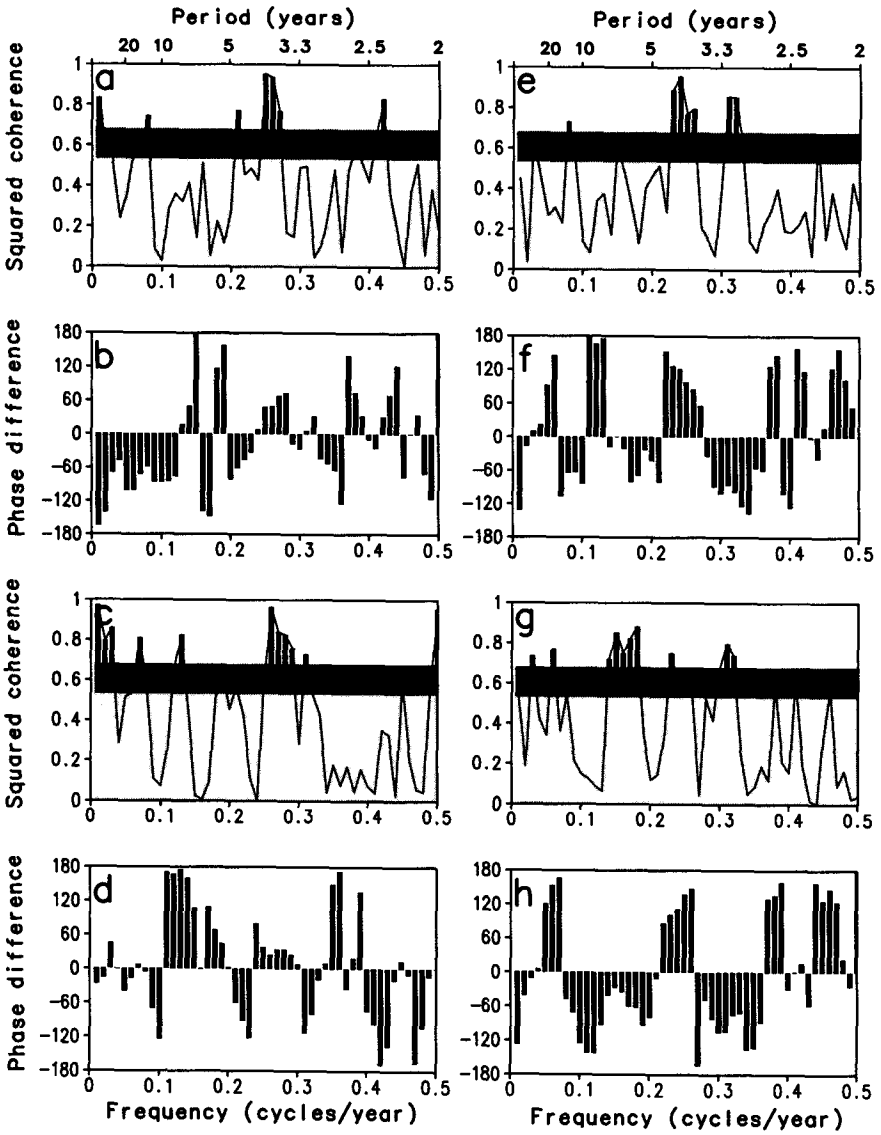

FIG. 9. Squared coherence and phase difference between the Northern and Southern Hemisphere SST time series. Panels (a)–(d) are for the observed GOSTA time series, and (e)–(h) are for the GFDL coupled model time series. In (a), (c), (e), and (g), the solid line is the estimated squared-coherence, the lighter shading is the 95% significance level, the darker shading is the 99% significance level, and the black bars denote the squared coherence that exceeds the 99% level. In (b), (d), (f), and (h), dark bars denote phase difference. Approximate locations of the subregion time series are (a) and (b) 5°W–5°E, 15°–25°S and 25°–65°W, 15°–25°N, (c) and (d) 5°W–5°E, 15°–25°S and 25°–55°W, 5°–15°N, (e) and (f) 6°W–6°E, 16°–25°S and 24°–66°W, 16°–25°N, and (g) and (h) 6°W–6°E, 16°–25°S and 24°–54°W, 7°–16°N.

tropical North Atlantic for cross-spectral analysis resulted in similar conclusions.

The above results of spectral and cross-spectral analyses, albeit limited by the availability of only a few, 100-yr long, observed SST time series, suggest that there is a large amount of decadal variability in each hemisphere. Spectral and cross-spectral analyses of the time series for the corresponding subregions in the GFDL coupled model also point generally toward the two types of decadal timescale variability in the two hemispheres. The dominant decadal timescales implied by the peaks in the Fourier spectra (Fig. 4) and the T-EOFs from the SSA analysis (Fig. 6), and the peaks in squared coherence (Fig. 9), however, are not located at the same timescales. This implies that the amplitudes of the coherent (between the two hemispheres) decadal timescale variability are not as large as the amplitudes of the independent decadal timescale variability in each

hemisphere. So, it seems that there may be two types of decadal variability in the GOSTA and GFDL SST datasets: (a) independent in each hemisphere, and (b) highly coherent with approximately opposite phases between the two hemispheres. Scarcity of reliable 100-yr observed SST time series over large parts of the tropical Atlantic inhibits further investigation of the spatial structures of the observed decadal timescale SST variability. That problem, however, is not present for the GFDL model dataset. The analysis of spatial structures of decadal timescale SST variability in the GFDL coupled model is described in the next section.

6. Analysis of spatial structures of model SST variability

In the previous section, analyses of decadal variability in time series of the observed and model SST in a few subregions were described. Since 100-yr monthly average and annual-average model SST time series are available on a regular grid spanning global oceans, they were used for detailed analyses of the spatial structures of decadal timescale SST variability in the GFDL coupled model's tropical Atlantic region. The FSA and EOF analyses techniques, described in section 4, were used. Results of the analyses are described and discussed in this section.

a. Frequency-domain analysis

Indications of frequency-dependent connections between the decadal variability in the tropical North and South Atlantic, based on the earlier described analyses of a few observed and model SST time series, motivated us to analyze spatial structures of decadal timescale variability as functions of oscillation frequency. Cross spectra between the SST anomaly time series at a reference grid point and at all grid points over the tropical Atlantic Ocean were estimated. Contour maps of squared coherence and phase difference, along with the 95% and 99% confidence levels, were plotted for each Fourier period from 8.3 to 20 yr. Such calculations were carried out for several reference grid points in the tropical North and South Atlantic. The general characteristic of the squared-coherence maps is that oscillations are highly coherent only within each tropical hemisphere for periods shorter than 11.1 yr. For periods between 11.1 and 20 yr, oscillations are highly coherent over both tropical hemispheres with typical interhemispheric phase differences of 150°–180°. Representative contour maps of squared coherence and phase difference for a reference grid point at 2°E–16°S are shown in Fig. 11 for 8.3- and 16.6-yr periods.

Thus, frequency-domain correlation analysis reveals two types of spatial structures within the decadal timescale band of 8.3–20 yr. Contour maps of fractional variance of annual-average SST anomalies (not shown) in the 8.3–11.1-yr and 12.5–16.6-yr bands show that the fractional variance in the former band is approximately 20%, whereas that in the latter band is approximately 10%. This implies that the independent decadal timescale variability in each hemisphere is twice as strong as the decadal timescale variability that is highly coherent between the two hemispheres. As described in section 5, the analyses of the GOSTA SST time series also point toward the same conclusion. The suggestion of approximately opposite phases of SST variability at multidecadal timescales is also present in the results of the singular spectrum analysis. It must be pointed out that a 100-yr time series has only a few Fourier frequencies at the decadal and longer timescale end of the spectrum. Therefore, the relationship between frequency and spatial structure in these 100-yr datasets is only approximate.

To look at the spatial structures of SST variability from the point of view of time-domain correlation analysis, correlation coefficients between a reference grid point and all grid point SST anomaly time series were calculated. Correlation coefficients between grid points were also calculated for SST time series filtered with a bandpass of 8.3–11.1 yr (four Fourier frequencies). If the bandpass filter is not applied, the correlation (not shown) between SST variability in the Northern and Southern Hemispheres in the tropical Atlantic is insignificantly small. Correlation (not shown) among filtered time series is larger and reveals cross-equatorial variability at decadal timescales, but the reduced number of independent samples in the filtered time series throws considerable doubt on the statistical significance of the correlation. Composite analyses of SST anomaly maps also resulted in similar conclusions. Extrema of the various phases of time series over the tropical North and South Atlantic were used to prepare the composite maps from SST anomaly maps. Although some of the composite maps (not shown) do show weak cross-equatorial patterns, the amplitudes of the composite anomalies are not significantly large. The time-domain analyses thus confirm the results of the frequency-domain analyses.

b. Empirical orthogonal function analysis

EOF analysis has been used extensively in isolating empirical modes of climate variability and was used in most of the earlier-cited studies of tropical Atlantic SST variability. We used EOF analysis in several different forms, explained in section 4, to isolate dominant empirical modes of variability of tropical Atlantic SST, to compare with the earlier described analyses of relatively short time series of SST observations, and for better interpretation of the results of our analyses.

We calculated EOFs and PCs of the tropical Atlantic SST anomalies from the GFDL coupled model dataset, using the conventional EOF analysis technique in which covariances between time series at various grid

points are used (referred to as E1). We also calculated EOFs and PCs using the space–time interchange technique (see section 4) but without subtracting the domain-average SST anomaly (referred to as E2). Both these techniques yielded approximately similar looking EOFs and PCs (not shown), with the first EOF pattern having the same sign over the entire tropical Atlantic and the second EOF pattern having opposite signs in the tropical North and South Atlantic. The PC time series associated with the second EOFs show the presence of significant decadal variability.

Using the EOF technique in which domain-average anomalies were subtracted from the gridpoint anomalies at each point in time (referred to as E3), we then performed calculations with two sampling intervals (monthly average and annual average), three domain extents (20°S–20°N, 29°S–29°N, and 47°S–47°N), and two types of SST anomaly time series (anomalies with respect to time and space averages, and the same anomalies normalized by the standard deviation of the time series at each grid point). The variety of approaches (12 sets of EOF analyses) provides an assessment of the stability of the results. The number of independent samples in each EOF 1 time series was estimated from the decay of the lagged-autocorrelation function. Thirty-three and 100 independent samples were assumed, based on the decay of lagged-correlation functions, to estimate sampling errors for EOFs of annual average (100 total samples) and monthly average (1200 total samples) data, respectively. Tables 2 and 3 show percent variances contained in the first two EOFs calculated with annual average and monthly average time series, respectively. Comparison of the two tables shows that the percent variance contained in each EOF is larger when annual average time series were used. The comparison also shows that the percent variance contained in each of the EOFs calculated with SST anomalies, which were not normalized, is approximately the same as the corresponding EOFs calculated with normalized SST anomalies. The percent variance contained in the first EOF in each of the analyses decreases as the latitudinal extent of the EOF calculations is increased from 20°S–20°N to 47°S–47°N. Also, according to North et al.'s (1982) criterion, the first and second EOFs of annual average and monthly average data for the domain 47°S–47°N are not independent. Therefore, it appears that the latitudinal coherence of the phenomenon captured by the first EOFs is confined to tropical latitudes.

The spatial patterns of the first PCs from all 12 analyses using technique E3 are generally similar. Therefore, only the first PC, the EOF, the estimated spectrum of the EOF time series, and the explained percent variance by the first EOF at each grid point from annual average SST data between 20°S and 20°N are shown in Fig. 12. The first EOF of annual-average SST anomalies without normalization contain 20.5% ± 5.0% variance. The PC pattern in Fig. 12a shows cross-equatorial SST variability between 20°S and 20°N. The EOF 1 time series (Fig. 12b) shows variability at various timescales, but as the corresponding spectrum (Fig. 12c) shows, the dominant peaks are at timescales of approximately 10 yr and 35–40 yr. There are also secondary peaks between timescales of approximately 2.8 and 4.5 yr. Comparison with the equivalent red noise spectra in Fig. 12c shows that the decadal, multidecadal, and the 2.8–4.5-yr peaks are statistically significant at the 99% confidence level. Figure 12d shows the coefficient of variation between the EOF 1 time series and each gridpoint time series. Variation due to EOF 1 explains approximately 40% of the total variation in southeastern tropical Atlantic SST, and approximately 20% of the total variation in the south-central and north-central tropical Atlantic SSTs. The typical peak-to-peak amplitude of decadal variability in Fig. 12b is approximately 1–1.5 K, whereas the maximum linear trend of SST in the model's tropical

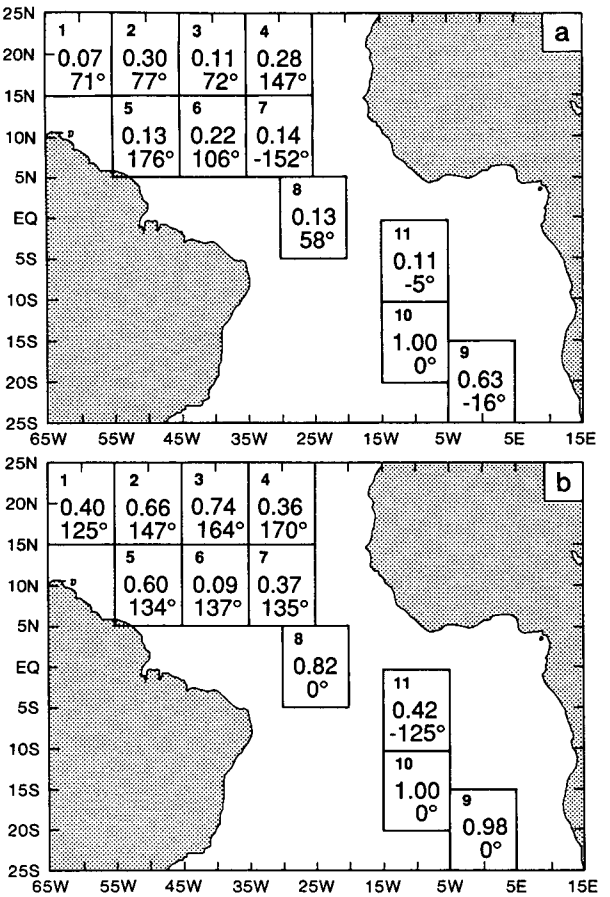

FIG. 10. Squared coherence and phase difference between the GOSTA SST time series at a reference grid box centered at 10°W, 15°S and other grid boxes over the tropical Atlantic Ocean. (a) The squared coherence and phase difference, respectively, at the 8-yr period, and (b) the squared coherence and phase difference, respectively, at the 12.5-yr period.

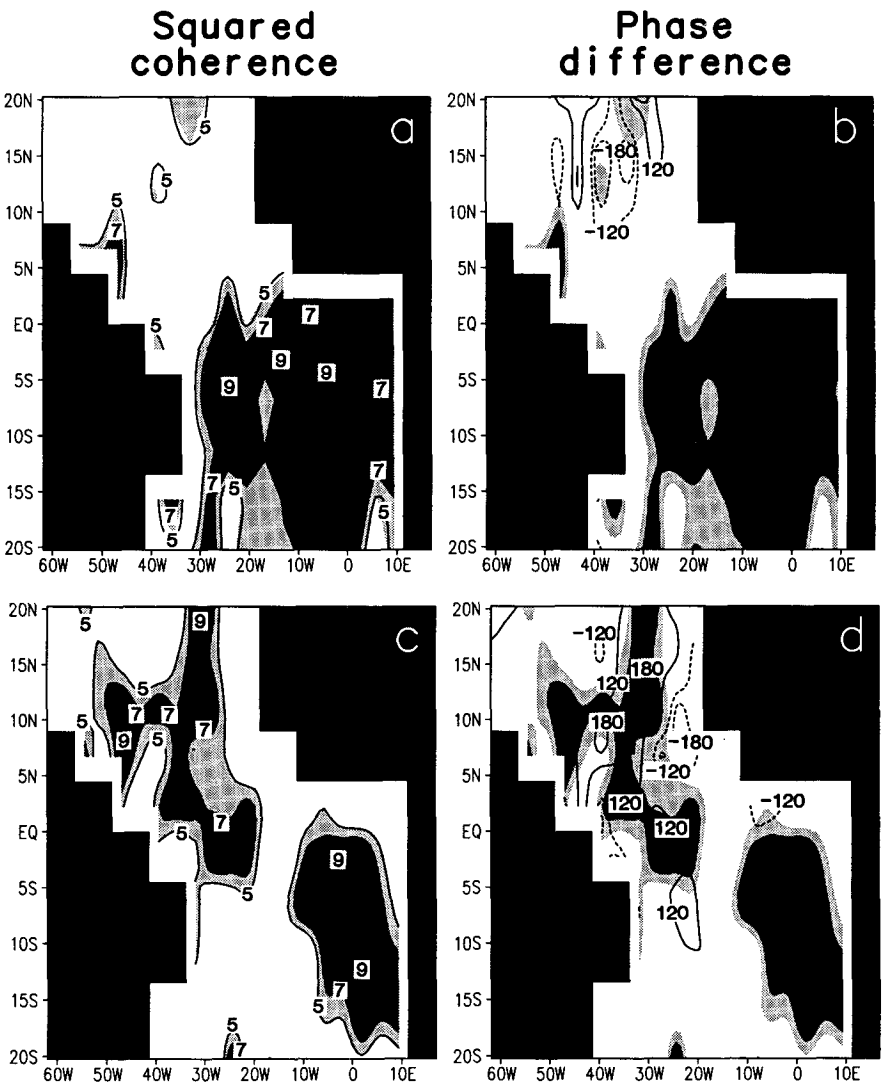

FIG. 11. Squared coherence, multiplied by 10, and phase difference between the SST time series at a reference grid point (2°E, 16°S) and all other grid points over the tropical Atlantic Ocean of the GFDL coupled model. Light shading indicates the 95% confidence level and dark shading indicates the 99% confidence level. Panels (a) and (b) are the squared coherence and phase difference, respectively, at the 8-yr period, and (c) and (d) are the squared coherence and phase difference, respectively, at the 16-yr period.

TABLE 2. Percent variances in empirical orthogonal functions of annual-averge time series, with percent sampling errors in parentheses.

	Data without normalization		Data with normalization	
	EOF 1	EOF 2	EOF 1	EOF 2
20°S–20°N	20.5 (5.0)	10.6 (2.6)	18.7 (4.6)	8.3 (2.0)
29°S–29°N	14.9 (3.6)	9.0 (2.2)	14.7 (3.6)	8.8 (2.1)
47°S–47°N	10.2 (2.5)	9.3 (2.3)	10.5 (2.6)	8.4 (2.0)

TABLE 3. Percent variances in empirical orthogonal functions of monthly average time series, with percent sampling errors in parentheses.

	Data without normalization		Data with normalization	
	EOF 1	EOF 2	EOF 1	EOF 2
20°S–20°N	14.8 (2.1)	9.9 (1.4)	13.9 (2.0)	7.8 (1.1)
29°S–29°N	11.5 (1.6)	8.0 (1.1)	11.0 (1.5)	7.0 (1.0)
47°S–47°N	9.1 (1.3)	6.8 (1.0)	8.8 (1.2)	6.3 (0.9)

Atlantic (Fig. 3b) is only 0.02 K/10 yr. Thus, the contribution from the decadal variability to SST changes in the tropical Atlantic is much larger than the contribution from model climate drift during the 100-yr period of the analyses.

Comparison of the PC pattern in Fig. 12a with EOFs of the observed SST anomalies calculated by, among others, Weare (1977), Hastenrath (1978), Lough (1986), Semazzi et al. (1988), Houghton and Tourre (1992), and Ward and Folland (1991) shows that the PC pattern in Fig. 12a is similar to the second EOFs in the above-cited analyses of the observed SST. The PC pattern in Fig. 12a is also similar to the cross-equatorial bipolar patterns that appeared as second EOF when we used the earlier described techniques E1 and E2. This comparison of results of the three EOF analyses are helpful in the interpretation of the north–south EOF pattern. The domain-average SST anomaly time series is an accurate representation of the PC time series associated with the first EOF pattern, with the same sign over the entire tropical Atlantic domain and approximately the same magnitude, from the EOF analyses E1 and E2. In EOF analysis E3 (in which domain average SST anomalies were subtracted at each point in time), the second EOF pattern of E1 and E2 appears as the first EOF. Subtraction of domain-average SST anomalies in our EOF analysis technique facilitates the interpretation of the cross-equatorial pattern as oscillations of the approximately southeast–northwest SST gradient. This is further illustrated in Fig. 13 with two time series representative of the SST variability in the tropical North and South Atlantic, respectively. The two representative time series (Fig. 13a) do not appear to be highly correlated. After the average time series

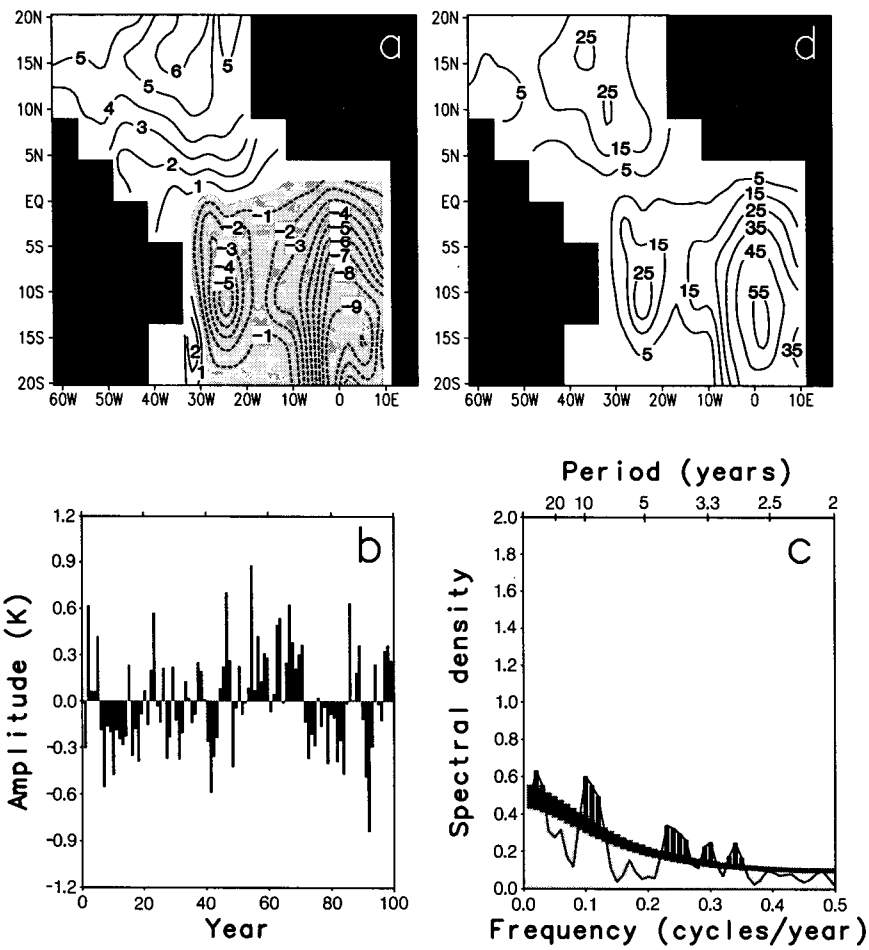

FIG. 12. Empirical orthogonal function analysis over the domain 20°S–20°N. Annual average sea surface temperature anomalies in the GFDL coupled model were used. (a) First principal component multiplied by 10, (b) first EOF amplitude (K) time series; (c) estimated spectrum (solid line) of the first EOF amplitude time series, equivalent red noise spectrum (lighter shading), the red noise spectrum (darker shading) that peaks in the EOF spectrum must exceed for significance at the 99% level, and the significant spectral estimates (dark bars); and (d) percent of the total variance "explained" by EOF 1. All spectral estimates are in K^2 per unit frequency.

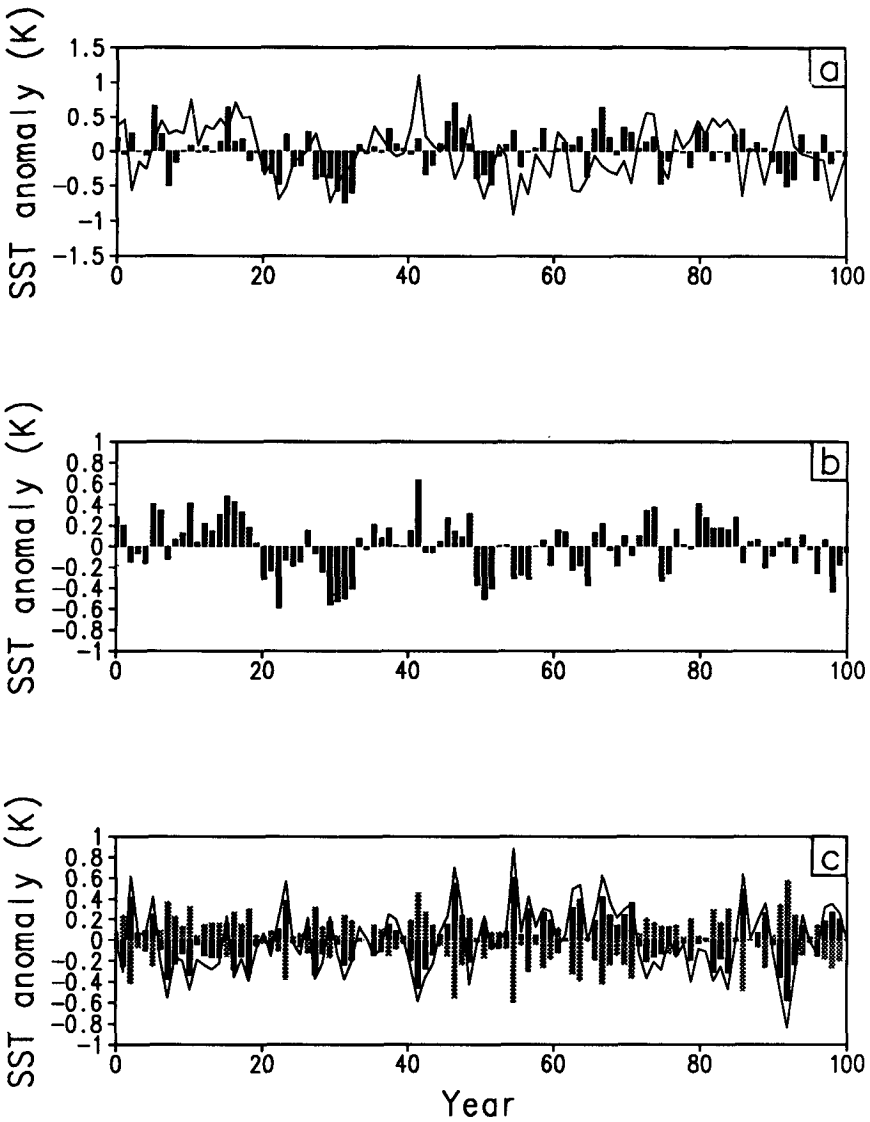

FIG. 13. (a) Representative time series of the tropical North Atlantic (NH) (dark bars) and South Atlantic (SH) (solid line) SST anomalies, (b) average time series of the two representative time series, and (c) the difference time series between the NH (dark bars) and SH (light bars) time series and the average time series, and the tropical Atlantic EOF 1 time series (solid line) from Fig. 12b.

(Fig. 13b) of the two representative time series is subtracted from each of them, the resultant two anomaly (with respect to the domain average) time series (Fig. 13c) have equal magnitudes and exactly opposite phases. The first EOF time series (Fig. 12b) is also plotted in Fig. 13c and shows that it almost exactly matches the two anomaly time series representative of the tropical North and South Atlantic SST variability.

Therefore, it appears that even though the decadal timescale variability is largely incoherent between the tropical North and South Atlantic SST, the approximately southeast–northwest SST gradient appears to vary at decadal timescales and that the cross-equatorial pattern should be interpreted as the pattern of variability of the SST gradient. Since the atmosphere responds to SST gradients, it is not surprising that variability of the tropical Atlantic SST gradient (as represented by the southeast–northwest EOF pattern) was found to be correlated with atmospheric phenomena in the vicinity of the tropical Atlantic region in previous studies [see, for example, Hastenrath and Greischar (1993)].

7. Concluding remarks

Fourier and singular spectrum analyses of 100-yr observed SST time series from the Global Ocean Sur-

face Temperature Atlas (GOSTA) representing 11 subregions, each 1×10^6 km^2 area, of the tropical Atlantic Ocean showed that statistically significant decadal timescale variability with typical amplitudes of 0.2–0.4 K exists in the observed, uncorrected, and corrected SST time series. The decadal variability is much stronger in the tropical South Atlantic than in the tropical North Atlantic. Spectral and cross-spectral analyses showed that there appear to be two types of decadal variability in the observed SST time series: (a) independent variability in the tropical North and South Atlantic at timescales between approximately 8 and 11 yr, and (b) highly coherent variability with opposite phases between the two hemispheres at timescales between approximately 12 and 20 yr. Variability of the first type was stronger than that of the second type in the observed SST time series. The spectral analyses also revealed multidecadal variability of the tropical North and South Atlantic SST, with approximately opposite phases of variability between the two hemispheres. Analyses of 100-yr SST time series at the corresponding subregions in the GFDL coupled ocean–atmosphere model pointed toward generally similar conclusions as from the analyses of the observed SST time series. The GFDL coupled model, however, simulates the decadal–multidecadal variability at somewhat shorter timescales. The decadal timescale variability had maximum amplitudes in the tropical northwest and southeast Atlantic Ocean in both the observed and model SST time series. The detection of multidecadal variability should not be considered quantitatively definitive since the GOSTA and GFDL model SST time series analyzed in this work span only 100-yr periods.

The application of a variant of conventional EOF analysis technique showed that a pattern of decadal variability with opposite polarities in the Northern and Southern Hemispheres appears as the first PC-EOF, statistically independent from subsequent PC-EOF pairs. Contrary to the results of this variant of the EOF analysis, the results obtained with two other variants of the EOF analysis technique, gridpoint correlations, composite analyses, and Fourier cross-spectrum analysis did not show significant cross-equatorial variability. An explanation of the contradictory results was provided, suggesting that the bipolar PC pattern and the associated timescale of approximately 10 yr should be interpreted as variability of the interhemispheric gradient of SST anomalies. The timescale of variability of the interhemispheric SST gradient implied by the results of the EOF analyses is shorter than that of the interhemispheric variability of SST anomalies shown by cross-spectral analyses. The former interhemispheric variability is substantially stronger than the latter.

The scarcity of observed SST time series of sufficient length and reliability over large parts of the tropical Atlantic Ocean prevented us from conducting detailed analyses of the spatial structures of the observed decadal and multidecadal timescale variability. It is clear, however, that the GFDL coupled model, while employing relatively simple physical parameterizations and coarse spatial resolutions, simulates reasonably well the patterns, amplitudes, and timescales of the decadal and multidecadal variability inferred from the available SST observations. Thus, very fine spatial resolution and complex physical parameterizations do not appear to be essential to simulate this decadal–multidecadal timescale variability. The decadal and multidecadal timescale variability of the tropical Atlantic SST, both the actual (to the extent represented in the GOSTA dataset) and in the GFDL model, stand out significantly above the background red noise, suggesting that specific sets of processes may be responsible for the choice of the decadal and multidecadal timescales. Preliminary analysis of the GFDL coupled model output indicates that perturbations in heat transport in the model's Atlantic Ocean and ocean–atmosphere interaction play major roles in the decadal–multidecadal variability of the model's tropical Atlantic SST. It must be emphasized that the GFDL coupled ocean–atmosphere model generates the decadal–multidecadal timescale variability without any externally applied force, solar or lunar, at those timescales. In the earlier cited work (Mehta 1991, 1992, 1994) with idealized ocean–atmosphere models, decadal–multidecadal variability occurs as normal modes of oscillation of the coupled ocean–atmosphere mean meridional circulations. Comprehensive analyses of the GFDL coupled model output and results from the idealized ocean–atmosphere models are in progress to study and compare the mechanisms of decadal–multidecadal timescale variability in the idealized and GFDL coupled ocean–atmosphere models.

Preliminary analyses of other quantities in the GFDL coupled model show that a substantial amount of climate variability is associated with the SST variability described in the present paper. Comprehensive analyses of the model quantities and comparison of the results with available observations are in progress. The results of the above analyses will be presented in subsequent papers.

Flux adjustments employed in the GFDL coupled model maintain the model SST climatology close to the observed SST climatology. If the mean climate plays a crucial role in generating decadal–multidecadal variability, as the work with idealized ocean–atmosphere models indicates, then maintenance of the model SST climatology (and perhaps of other model quantities also) close to the observed would be conducive to a better simulation of decadal–multidecadal variability by the GFDL coupled model. If the decadal–multidecadal variability is generated as a subharmonic of the annual cycle of insolation acting on the coupled ocean–atmosphere system, then the flux adjustments would have a more direct role in the generation of this variability since the adjustments have substantially large annual cycles. It is impossible, however, to gauge

the effect of flux adjustments on the variability described in this paper without further experimentation with the GFDL and other such coupled ocean–atmosphere models.

Acknowledgments. The authors would like to express their deep appreciation to S. Manabe and R. J. Stouffer for the use of their model output and to K.-M. Lau for supporting this work. The authors are grateful to K. Bryan, S. Hastenrath, R. Houghton, S. Manabe, A. Mehta, R. Livezey, F. Semazzi, and three anonymous reviewers for carefully reading earlier versions of the manuscript and making useful suggestions. One of the authors (VM) would like to thank R. F. Cahalan for several illuminating discussions about EOF analysis, and the authors would also like to thank Mike Fiorino and Brian Doty for their help in using the graphics software package GrADS, and Ms. Laura Rumburg for drafting the illustrations. This work was partially supported by NOAA's Atlantic Climate Change Program Grant NA93AANAGO349.

REFERENCES

Bloomfield, P., 1976: *Fourier Analysis of Time Series: An Introduction.* John Wiley and Sons, 258 pp.

Bottomley, M., C. K. Folland, J. Hsiung, R. E. Newell, and D. E. Parker, 1990: *Global Ocean Surface Temperature Atlas (GOSTA).* Her Majesty's Stationary Office.

Bryan, K., 1969: Climate and the ocean circulation: III. The ocean model. *Mon. Wea. Rev.,* **97,** 806–827.

——, and L. J. Lewis, 1979: A water mass model of the world ocean. *J. Geophys. Res.,* **84**(C5), 2503–2517.

——, 1987: Potential vorticity in models of the ocean circulation. *Quart. J. Roy. Meteor. Soc.,* **113,** 713–734.

Folland, C. K., T. N. Palmer, and D. E. Parker, 1986: Sahel rainfall and worldwide sea temperatures. *Nature,* **320,** 602–606.

——, J. A. Owen, M. N. Ward, and A. W. Colman, 1991: Prediction of seasonal rainfall in the Sahel region using empirical and dynamical methods. *J. Forecasting,* **10,** 21–56.

Ghil, M., and R. Vautard, 1991: Interdecadal oscillations and the warming trend in global temperature time series. *Nature,* **350,** 324–327.

Gilman, D. L., F. J. Fuglister, and J. M. Mitchell Jr., 1963: On the power spectra of "red noise." *J. Atmos. Sci.,* **20,** 182–184.

Gordon, C. T., and W. Stern, 1982: A description of the GFDL global spectral model. *Mon. Wea. Rev.,* **110,** 625–644.

Hastenrath, S., 1978: On modes of tropical circulation and climate anomalies. *J. Atmos. Sci.,* **35,** 2222–2231.

——, 1990: Decadal-scale changes of the circulation in the tropical Atlantic sector associated with Sahel drought. *Int. J. Climatol.,* **10,** 459–472.

——, and L. Greischar, 1993: Circulation mechanisms related to northeast Brazil rainfall anomalies. *J. Geophys. Res.,* **98,** 5093–5102.

Houghton, R. W., and Y. M. Tourre, 1992: Characteristics of low-frequency sea surface temperature fluctuations in the tropical Atlantic. *J. Climate,* **5,** 765–771.

Levitus, S., 1982: *Climatological Atlas of the World Ocean,* NOAA Prof. Paper No. 13, U.S. Dept. of Commerce, 173 pp.

Lough, J. M., 1986: Tropical Atlantic sea surface temperature and rainfall variations in sub-Saharan Africa. *Mon. Wea. Rev.,* **114,** 561–570.

Manabe, S., and R. Stouffer, 1988: Two stable equilibria of a coupled ocean–atmosphere model. *J. Climate,* **1,** 841–866.

——, R. J. Stouffer, M. J. Spelman, and K. Bryan, 1991: Transient responses of a coupled ocean–atmosphere model to gradual changes of atmospheric CO_2. Part I: Annual mean response. *J. Climate,* **4,** 785–818.

Mehta, V. M., 1991: Meridional oscillations in an idealized ocean-atmosphere system, Part I: Uncoupled modes. *Climate Dyn.,* **6,** 49–65.

——, 1992: Meridionally propagating interannual-to-interdecadal variability in a linear ocean–atmosphere model. *J. Climate,* **5,** 330–342.

Moura, A. D., and J. Shukla, 1981: On the dynamics of drought in northeast Brazil: Observations, theory, and numerical experiments with a general circulation model. *J. Atmos. Sci.,* **38,** 2653–2675.

Nicholson, S. E., and B. S. Nyenzi, 1990: Temporal and spatial variability of SSTs in the tropical Atlantic and Indian Oceans. *Meteor. Atmos. Phys.,* **42,** 1–17.

North, G. R., T. L. Bell, R. F. Cahalan, and F. J. Moeng, 1982: Sampling errors in the estimation of empirical orthogonal functions. *Mon. Wea. Rev.,* **110,** 75–82.

Orszag, S. A., 1970: Transform method for the calculation of vector-coupled sums: Application to the spectral form of the vorticity equation. *J. Atmos. Sci.,* **27,** 890–895.

Penland, C., M. Ghil, and K. M. Weickmann, 1991: Adaptive filtering and maximum entropy spectra with application to changes in atmospheric angular momentum. *J. Geophys. Res.,* **96,** 22 659–22 671.

Semazzi, F. H. M., V. M. Mehta, and Y. C. Sud, 1988: An investigation of the relationship between sub-Saharan rainfall and global sea surface temperatures. *Atmos.-Ocean,* **26,** 118–138.

Servain, J., 1991: Simple climate indices for the tropical Atlantic Ocean and some applications. *J. Geophys. Res.,* **96,** 15 137–15 146.

Spiegel, M. R., 1961: Theory and problems of statistics. *Schaum's Outline Series in Mathematics,* McGraw-Hill, 359 pp.

Vautard, R., and M. Ghil, 1989: Singular spectrum analysis in nonlinear dynamics with applications to paleoclimatic time series. *Physica D,* **35,** 395–424.

Ward, M. N., and C. K. Folland, 1991: Prediction of seasonal rainfall in the north nordeste of Brazil using eigenvectors of sea-surface temperature. *Int. J. Climatol.,* **11,** 711–743.

Weare, B. C., 1977: Empirical orthogonal analysis of Atlantic Ocean surface temperature. *Quart. J. Roy. Meteor. Soc.,* **103,** 467–478.